Streptozotocin-Induced Dynamic Metabonomic Changes in Rat Biofluids

ARTICLE *in* JOURNAL OF PROTEOME RESEARCH · MAY 2012

Impact Factor: 4.25 · DOI: 10.1021/pr300280t · Source: PubMed

8 AUTHORS, INCLUDING:

Junfang wu
Wuhan Institute of Physics and Mathematics
14 PUBLICATIONS **229** CITATIONS
SEE PROFILE

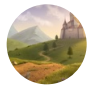

Hao Fuhua
Wuhan Institute of Physics and Mathematics
27 PUBLICATIONS **690** CITATIONS
SEE PROFILE

Yulan Wang
Chinese Academy of Sciences
123 PUBLICATIONS **4,783** CITATIONS
SEE PROFILE

Huiru Tang
Fudan University
167 PUBLICATIONS **4,941** CITATIONS
SEE PROFILE

Journal of proteome research

Article

pubs.acs.org/jpr

Streptozotocin-Induced Dynamic Metabonomic Changes in Rat Biofluids

Wenxin Xu,[†,§] Junfang Wu,[†] Yanpeng An,[†] Chaoni Xiao,[†,‡] Fuhua Hao,[†] Hongbing Liu,[†] Yulan Wang,[†] and Huiru Tang*[,†]

[†]State Key Laboratory of Magnetic Resonance and Atomic and Molecular Physics, Wuhan Centre for Magnetic Resonance, Wuhan Institute of Physics and Mathematics, Chinese Academy of Sciences, Wuhan 430071, People's Republic of China

[‡]College of Life Sciences, Northwest University, Xi'an 710069, People's Republic of China

[§]Graduate School of the Chinese Academy of Sciences, Beijing 100049, People's Republic of China

Supporting Information

ABSTRACT: Diabetes mellitus is a complex polygenic disease caused by gene-environment interactions with multiple complications, and metabonomic analysis is crucial for pathogenesis, early diagnosis, and timely interventions. Here, we comprehensively analyzed the dynamic metabolic changes in rat urine and plasma, which were induced by the well-known diabetogenic chemical streptozotocin (STZ), using ^{1}H NMR spectroscopy in conjunction with multivariate data analysis. The results showed that a single intraperitoneal injection of STZ with a moderate dosage (55 mg/kg) induced significant urinary metabonomic changes within 24 h. These changes showed time-dependence and heterogeneity among the treated animals with an animal recovered within 11 days. STZ-induced metabonomic alterations were related to suppression of glycolysis and TCA cycle, promotion of gluconeogenesis and oxidation of amino acids, alterations in metabolisms of basic amino acids associated with diabetic complications, and disruption of lipid metabolism and gut microbiota functions. With diffusion-edited NMR spectral data, we further observed the STZ-induced significant elevation of monounsaturated fatty acids and total unsaturated fatty acids together with reductions in PUFA-to-MUFA ratio in the blood plasma. These findings provided details of the time-dependent metabonomic changes in the progressive development of the STZ-induced diabetes mellitus and showed the possibility of detecting the biochemical changes in the early stage of type 1 diabetic genesis.

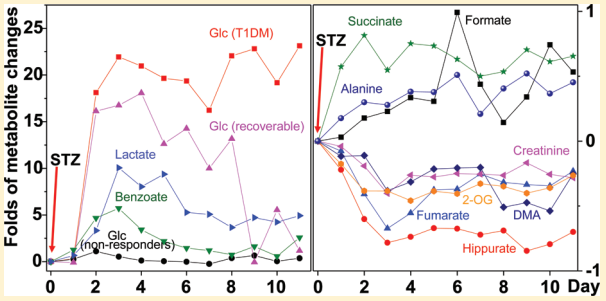

KEYWORDS: *metabonomics, diabetes, unsaturated fatty acids, ^{1}H NMR spectroscopy, multivariate data analysis*

INTRODUCTION

Diabetes is a rapidly growing polygenic complex disease in both the developed and developing world leading to morbidity and further life-threatening complications.[1] Such complications include macrovascular conditions, such as coronary heart disease and strokes, and microvascular problems for many functional organs, such as diabetic nephropathy, diabetic retinopathy, and even erectile dysfunction.[2] These complications often have already started and probably developed to some degree at the time point of diabetes diagnosis. World Health Organization (WHO) estimates that over 170 million people worldwide suffer from diabetes, and this number is likely to be doubled by 2030.[3] The importance and seriousness of the diabetic diseases have prompted many large-scale diabetes epidemiological studies throughout the world in order to understand the etiology and risk factors. These include the Diabetes Control and Complications Trial (DCCT) and Epidemiology of Diabetes Interventions and Complications (EDIC),[4] United Kingdom Prospective Diabetes Study (UKPDS),[5] Action in Diabetes and Vascular disease: preterAx and diamicroN MR Controlled Evaluation (ADVANCE).[6,7]

The current clinical diagnosis for diabetes relies on the measurements of either fasting plasma glucose (≥7.0 mmol/L), 2 h plasma glucose (≥11.1 mmol/L), or random plasma glucose (≥11.1 mmol/L) with symptoms of either hyperglycemia or hyperglycemic crisis or elevation of glycated hemoglobin (HbA1c, ≥6.5%).[8] However, such measurements often reflect the consequences of glucose metabolism dysfunction, and by then, the detriments and burdens of clinical diabetes are probably beyond retrieval. The detection of systems changes at the early stage of pathogenesis is thus vital in the context of preventative diagnosis, which requires holistic methods.

Systems approaches developed during past decades, such as genomics, transcriptomics, proteomics, and metabonomics methods, have important roles to play in understanding the pathogenesis and progression of diabetes since diabetes results from gene−environment interactions.[9] There are mainly two types of diabetes, namely, type 1 and type 2 diabetes, both of which are partially inheritable. Type 1 diabetes mellitus

Received: March 21, 2012
Published: May 7, 2012

(T1DM) is mainly triggered by viral infections and less commonly by stressors or environmental exposure. The chromosomal regions significantly associated with T1DM include the human leukocyte antigen (HLA) region[10,11] on chromosome 6p21.3, the insulin gene region[12] on chromosome 11p15, and the cytotoxic T-lymphocyte-associated 4 gene (CTLA4) region[13] on chromosome 2q33. Proteomic studies have indicated that the cytokine interleukin (IL)-1β plays an essential role in the T1DM pathogenesis[14] mediated through induction of nitric oxide synthase (iNOS) and nitric oxide, although NO-independent mechanisms are also implicated.[15] For T2DM, strong predictors include the family history, an increased body-mass index, elevated liver-enzyme levels, and reduced insulin secretion and sensitivity.[16] Genome-wide researches showed that variants in many genes (such as TCF7L2, PPARG, FTO, KCNJ11, NOTCH2, WFS1, CDKAL1, IGF2BP2, SLC30A8, JAZF1, and HHEX) were significantly associated with the risk of T2DM.[16] Some proteomics studies showed that differential expressions of many proteins, such as GLUT2, DNAJC3, VAMP2, RAB3A, and PC1/3, were associated with the insulin-secretory defects and T2DM.[17] Other proteins were also found to be associated with islet dysfunction, including the unfolded response proteins (ERP72, ERP44, ERP29, PPIB, FKBP2, FKBP11, and DNAJB11), endoplasmic reticulum-associated degradation proteins (VCP and UFM1), and multiple proteins related to mitochondrial energy metabolism (NDUFA9, UQCRH, COX2, COX4I1, COX5A, ATP6V1B2, ATP6V1H, ANT1, ANT2, ETFA, and ETFB).[17] These findings strongly imply that the analyses of the whole metabolite complement (i.e., metabonome) ought to be a relevant and potentially powerful approach for understanding the metabolic changes associated with the pathogenesis and progression of diabetes.

Metabonomics detects, quantifies, and catalogues the metabolite complement (in mammalian biofluids, cells, tissues, and/or whole organisms), and its dynamic changes for the integrated biological systems so as to provide detailed molecular insights about pathophysiology in the systems level.[18−21] Subsequently, the effects of both endogenous factors (such as physiology and development) and exogenous factors (such as environmental factors) on the systems metabonome can be understood.[18−21] As a well-established metabonomic analysis tool,[21−23] the combination of ^{1}H NMR spectroscopy with multivariate statistical analysis techniques has already been widely applied to detect xenobiotic metabolites in biofluids[24] and the molecular aspects of stresses,[25] carcinogenesis,[26] and chemical and environmental toxicology.[27,28]

Such metabonomic investigations have also been used to understand the diabetes-related metabolic alterations in terms of endogenous and environmental factors. In fact, NMR studies of the human plasma and urine demonstrated the usefulness of metabolic profiling in this context as early as 1980s, revealing the altered blood glucose metabolism and ketogenesis for the diabetes patients.[29] Metabolic dysfunctions in fatty acids, organic acids, and phospholipids were found to be associated with diabetes and responsive to drug interventions.[30] Metabonomic analysis results from insulin-resistant mouse models further indicated the association of the gut microbiota with the phenotypic development of fatty liver[31] probably due to altered gut microbiota modulations on the host metabolisms.[32,33] More recently, many changes of human plasma metabonome were investigated for diabetic kidney diseases, insulin resistance, and the glucose challenge induced metabolic responses from the prediabetes.[34,35] Furthermore, human serum metabonomic changes were found to be correlated with the progressive development of glucose intolerance and insulin resistance severity.[36] Moreover, the dependence of diabetes-associated metabonomic changes on species and models has been reported in a comparative urinary metabonomic study on two rodent models (db/db mouse and obese Zucker rat) and untreated human T2DM patients.[37]

T1DM in humans is characterized by specific destruction of the pancreatic β-cells. When the symptom is apparent, there is little surviving β-cell mass and the disorder progresses to absolute insulinopenia.[38] For animal models, streptozotocin (STZ) has been used widely as a classical diabetogenic chemical in diabetes research[39] since STZ causes selective necrosis of pancreatic β-cells leading to a state of absolute insulinopenia[40] that is similar to T1DM in humans. Therefore, STZ-induced diabetic animal models are useful to study the metabonomic changes at the initial onset of the diabetic process and their association with the disease development. Some early studies have already indicated the feasibility of this model by showing that STZ causes changes in glucose metabolism and TCA cycle.[41]

These studies undoubtedly demonstrated the importance of endogenous and environmental factors in the development of diabetes with associated metabolic changes. However, these works were mostly focused either on the consequences resulting from diabetic conditions or the method developments for diabetes diagnosis. Few studies were designed to comprehensively understand the metabonomic alterations associated with the diabetic pathogenesis especially in the early onset stages[42] and the dynamic progression of the diseases. For the time being, the mechanistic aspects of the diabetes development remain largely unclear; early and preventative diabetes diagnostic methods remain to be developed.

In this study, we employed the well-known STZ-induced rat diabetes model with a moderate dose (55 mg/kg body weight) to deliberately avoid an excessive physiological reaction,[43] so as to obtain a gradual disease development process. We systematically analyzed the dynamic changes of the rat urinary and blood plasma metabonome throughout the time course of diabetes progression, especially the important variations in the early stage using ^{1}H NMR spectroscopy in conjunction with multivariate data analysis. The main objectives of this study are to (1) further characterize the heterogeneity of metabonomic changes induced with the moderate dose of STZ and (2) understand the manifested dynamic changes in both urinary and plasma metabonome associated with the pathogenesis with particular interests in the early onset stage and progression of diabetes.

MATERIALS AND METHODS

Chemicals

Analytical grade NaCl, $K_2HPO_4{\cdot}3H_2O$, and $NaH_2PO_4{\cdot}2H_2O$ were all purchased from Sinopharm Chemical Reagent Co., Ltd. (Shanghai, China), and analytical grade NaN_3 was purchased from Fuchen Chemical Reagent Company (Tianjin, China). Streptozotocin (STZ) was purchased from Sigma-Aldrich Inc. (St. Louis, MO), whereas D_2O (99.9% D) and sodium 3-trimethylsilyl [2,2,3,3-$^2H_4$] propionate (TSP) were bought from Cambridge Isotope Laboratories Inc. Phosphate buffer (K_2HPO_4/NaH_2PO_4, 1.5M, pH 7.4) prepared in D_2O containing 0.05% TSP and 0.1% NaN_3 (w/v) was used in urinary analysis for its low-temperature stability and good solubility.[44] The saline solution used for plasma analysis was

dx.doi.org/10.1021/pr300280t | J. Proteome Res. 2012, 11, 3423−3435

prepared in D_2O including 25% H_2O, 0.9% NaCl, and 0.04% NaN_3 (w/v).

Animal Handling and Biofluid Collection

Thirty SPF-grade male Wistar rats (8 wks old, 239 ± 16 g) were obtained from Experimental Animal Center of Huazhong University of Science and Technology. All animal experiments were carried out in accordance with the National Guidelines for Experimental Animal Welfare (MOST, PR China, 2006) at the Center for Animal Experiments, Wuhan University, which had full accreditation from the Association for Assessment and Accreditation of Laboratory Animal Care International (AAALAC Intl.). Animals were maintained at room temperature (20 ± 2 °C) with a humidity of 40−70% and artificial dark/light cycles from 20:00−08:00. All rats had free access to the certified standard chow and water. After 7 days acclimation, predose urine samples were collected with metabolic cages. After fasting for 16 h, 19 rats were randomly selected and injected intraperitoneally with a single dose (55 mg/kg of body weight) of STZ solution, which was freshly prepared in an ice bath in 0.9% saline with HCl acidification (0.08 M, pH = 4.5, ice bath). The remaining 11 rats were used as controls and injected with the same volume of vehicle. The random blood glucose was measured twice with a Super Glucocard TMII (GT-1640) (ARKRAY, Inc., Japan) at day 4 and 9 after STZ treatment. On the day 5 postdose, 5 rats in both the control (C group) and STZ-treated group (S group) were sacrificed following ether anesthetization, and blood samples were collected. On the day 12 after STZ treatment, the rest of the animals were sacrificed in the same manner. Following STZ-treatment, rat urine samples were collected daily (days 1−11) using metabolic cages with the body weight of each animal weighed. Urine collection tubes were added with one drop of sodium azide solution (1% w/v, about 40 μL) to inhibit the bacterial growth. Blood plasma samples were obtained by the centrifugation of blood at 4 °C with 1% heparin as anticoagulant. Another part of blood serum samples were also prepared (without anticoagulant) for clinical chemistry measurements. The pancreases were immediately removed for histopathological examinations. All the samples were snap-frozen in liquid nitrogen and stored at −80 °C until required for analyses.

Pancreas Histopathology

The typical pancreas tissues in the control and STZ-induced groups were fixed in 10% buffered formalin and then embedded in paraffin wax. Sections with the thickness of 5 μm were obtained with a microtome and then stained with the routine hematoxylin and eosin (H&E) method for assessments. These experiments were carried out by a qualified pathologist at the Pathology Department, Center for Animal Experiment of Wuhan University, as a paid service.

Clinical Chemistry

Blood urea nitrogen (BUN), creatinine (CREA), alanine aminotransferase (ALT), total protein (TP), albumin (ALB), total bile acids (TBA), triglycerides (TG), glucose (Glc), urea (UA), and HDL-C were measured in Biochemistry Laboratory of the Center for Animal Experiment of Wuhan University using a HITACHI 7080 Automatic Chemistry Analyzer (Hitachi, Ltd.).

NMR Spectroscopy of Biofluids

Blood plasma (400 μL) was mixed with saline (200 μL) solution containing 0.04% w/v sodium azide (to inhibit bacterial growth in the sample during NMR analysis). The mixture was centrifuged at 10 000 rpm for 10 min, and the supernatant (550 μL) was transferred into 5 mm NMR tubes, respectively. All ^{1}H NMR spectra of plasma were recorded on a Varian Inova 600 NMR spectrometer (operating at 599.905 MHz for ^{1}H) equipped with an inverse detection probe with a shielded *Z*-gradient. Three spectra were acquired for each sample including a one-dimensional NOESYPR1D spectrum using a standard pulse sequence (RD-90°-t_1-90°−t_m-90°-acq)[45] with t_1 of 2.8 μs, water-suppressed Carr−Purcell−Meibom−Gill (CPMG) spectrum using the standard pulse sequence (RD-90°-(τ-180°-τ)$_n$-ACQ], and diffusion-edited spectrum using the pulse sequence [RD-90°-G1-τ-180°-G2-τ-90°-Δ-90°-G3-τ-180°-G4-τ-90°-Te-90°-ACQ]. The 90° pulse length was adjusted to about 10 μs for each sample with the relaxation delay (RD) of 1 s. In NOESYPR1D experiment, the water resonance was suppressed with a weak continuous wave irradiation during RD and the mixing time, t_m, of 100 ms. CPMG spin−echo spectra were recorded using a relaxation time (2nτ) of 152.4 ms. Diffusion-editing spectra were obtained with the SINE shaped pulsed-field gradient with τ of 1 ms and Δ of 200 ms. For each sample, 64 transients were collected into 32 000 data points with a spectral width of 12019.23 Hz and thus an acquisition time of 1.36 s.

Each urine sample (550 μL) was mixed with 55 μL of phosphate buffer containing 0.05% TSP as chemical shift reference and 0.1% NaN_3 as the bacterial growth inhibitor. After centrifugation at 10 000 rpm for 10 min, the supernatant (500 μL) was transferred into 5 mm NMR tubes respectively. Urine spectra were acquired at 298 K on a Bruker AV III 600 MHz spectrometer equipped with an inverse cryoprobe using the standard NOESYPR1D sequence with a recycle delay of 4 s and a mixing time of 100 ms. For each sample, 32 transients were collected into 32 000 data points with a spectral width of 12019.23 Hz and an acquisition time of 1.36 s.

For resonance assignment purposes, two-dimensional (2D) NMR spectra were recorded on selected samples in the same fashion as previously reported,[46,47] which included ^{1}H−^{1}H correlation spectroscopy (COSY), ^{1}H−^{1}H total correlation spectroscopy (TOCSY), *J*-resolved spectroscopy (JRES), ^{1}H−^{13}C heteronuclear single quantum correlation (HSQC), and ^{1}H−^{13}C heteronuclear multiple bond correlation (HMBC) 2D NMR spectra. For COSY and TOCSY experiments, 48 transients for each of 108 increments were collected into 2048 data points with the spectral width of 10.5 ppm for both dimensions. TOCSY spectra were acquired using MLEV-17 as a spin-lock scheme with the mixing time of 80 ms. In HSQC, composite pulse broad band decoupling (globally alternating optimized rectangular pulses, GARP) was employed on ^{13}C dimension during the acquisition period. 184 scans with 2048 data points were acquired for each of 90 increments with spectral widths of 10.5 and 165.6 ppm for ^{1}H and ^{13}C dimension, respectively. HMBC experiments were carried out with gradient selection in phase-insensitive mode with a long-range coupling constant set to 6 Hz. The data were Fourier transformed into 2048 × 2048 matrices with appropriate apodization functions and forward linear prediction (with functions provided in TOPSPIN) for the evolution dimension.

Data Processing and Multivariate Data Analysis

The NMR spectra were processed using the software package TOPSPIN (V2.0, Bruker Biospin, Germany). For one-dimensional ^{1}H NMR data, the FIDs were multiplied by an

dx.doi.org/10.1021/pr300280t | J. Proteome Res. 2012, 11, 3423−3435

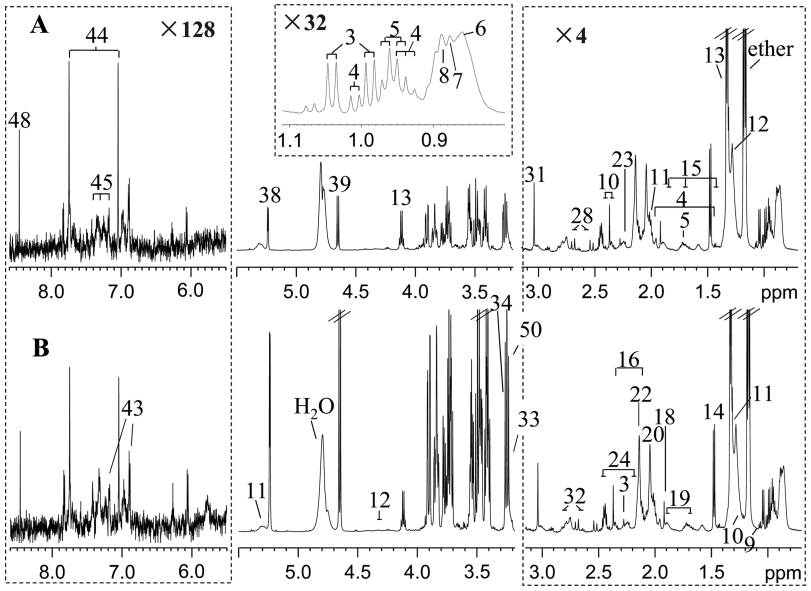

Figure 1. Typical 600 MHz CPMG spectra of plasma samples collected from a control rat (A) and a streptozotocin (STZ)-induced diabetic rat (B) at the fifth day after STZ-induction. The spectra in aromatic region δ 5.6−8.6 were vertically expanded 128 times, and the region δ 0.7−3.2 was expanded 4 times; the inset region δ 0.8−1.1 was expanded 32 times. The keys for metabolites are given in Table 1.

exponential weighting function with a line broadening factor of 1 Hz prior to FT. The spectra were then manually phase- and baseline-corrected and referenced to the chemical shift of the methyl resonance of lactate (δ 1.33) for plasma spectra and to TSP (δ 0.00) for urine samples.

The spectral region of δ 0−8.54 for plasma samples was divided into 8540 bins of equal width (0.001 ppm), whereas the region of δ 0.5−10 for urine samples was bucketed into 1900 buckets with the width of 0.005 ppm each using the AMIX software package (V3.8.3, Bruker Biospin). The spectral regions containing the water resonance (δ 4.662−5.23 for plasma and δ 5.22−4.70 for urine) were discarded from all data sets prior to normalization and multivariate data analysis in order to eliminate the effects of imperfect water suppression. For urine samples, the spectral regions containing urea resonance were also excluded (δ 6.02−5.425). For data normalization, we found that the plasma results from probabilistic quotient normalization (PQN) and no-normalization were not consistent with the clinical chemistry data for triglycerides. The NMR spectral regions were then normalized to the sum of spectrum to compensate for the overall concentration differences, and results for triglycerides were consistent with the clinical chemistry data.

Principal component analysis (PCA) was performed with the mean-centered data with the software package SIMCA-P$^+$ (V12.0, Umetrics, Sweden) to examine group clustering and to find possible outliers. Results were visualized in the form of the score plots, where each point represented an individual sample (or its metabonome), and loadings plots, where each coordinate represented one NMR spectral region (i.e., metabolite signal). The orthogonal projection to latent structure with discriminant analysis (OPLS-DA)[48,49] was further conducted with unit-variance scaling (UV) to identify metabolites significantly contributing to the group differentiation. The 7-fold (5-fold if $n < 6$) cross-validated OPLS-DA models were calculated with one predictive and one orthogonal component using the NMR data as X-matrix and the class information as Y-variables. The quality of the models was described by the parameters R^2X, representing the total explained variation, and Q^2, indicating the predictability of the models. These models were rigorously evaluated with the well-known CV-ANOVA approach with $p < 0.05$ as significant.

The loadings were calculated using the well-known back-transformation method.[48] The coefficient-coded loadings plots were generated with an in-house developed MATLAB script and were color-coded with the square of coefficients (r^2), where warm-colored (e.g., red) variables reflected more significant contribution to the classification than the cold-colored (e.g., blue) ones. In this study, appropriate correlation coefficients were used as the cutoff values (depending upon the number of animals used) for the statistical significance on the basis of the discrimination significance at the level of $p < 0.05$; such was determined according to the test for the significance of the Pearson's product-moment correlation coefficients.[48]

Dynamic metabolite changes were calculated for each time point in the forms of $[C_T - C_C]/C_C$ and $[C_N - C_C]/C_C$, where C_T, C_N, and C_C stood for the metabolite concentrations in STZ-induced diabetes group, nonresponders, and control group, respectively. Since metabolite concentration is directly proportional to the integral areas for metabolite signals in NMR, these ratios have been calculated from the integrals of selected metabolite signals (least overlapping ones) against these in the control group without obtaining the absolute concentrations for all metabolites.

STZ-induced changes in fatty acid composition were also calculated from the diffusion-edited spectra of blood plasma including the percentage of unsaturated fatty acids (UFA%), polyunsaturated fatty acids (PUFA%), and monounsaturated fatty acids (MUFA%) in all fatty acids. The PUFA-to-MUFA ratio (PUFA/MUFA) was also calculated. These calculations were based on the spectral integral areas for —C***H***═C***H***— (from UFA, δ 5.28), —C***H***$_3$ (from all fatty acids, δ 0.837), ═CH—C***H***$_2$—CH═ (from PUFA, δ 2.76) taking into consideration of proton numbers; the signal area for MUFA was calculated by subtracting that for PUFA from UFA.

dx.doi.org/10.1021/pr300280t | J. Proteome Res. 2012, 11, 3423−3435

Table 1. NMR Signal Assignments for Metabolites in Rat Plasma and Urine Samples

no.	metabolites	assignments	δ ^{1}H	biofluids[a]
1	α-keto-β-methyl-*N*-valerate	δCH_3, γCH_2, $\gamma' CH_2$	0.87(t), 1.72(m), 1.46(m)	U
2	butyrate	γCH_3, βCH_2, αCH_2	0.9(t), 1.56(m), 2.16(t)	U
3	valine	γCH_3, $\gamma' CH_3$, βCH, αCH	0.99(d), 1.04(d), 2.27(m), 3.61(d)	P
4	isoleucine	δCH_3, γCH_3, γCH_2, βCH, αCH	0.93(t), 1.00(d), 1.46(m), 1.97(m), 3.56(dd)	P
5	leucine	δCH_3, $\delta' CH_3$, γCH, αCH_2	0.94(d), 0.96(d), 1.71(m), 3.74(m)	P
6	HDL	$CH_3(CH_2)_n$	0.86(m)	P
7	LDL	$CH_3(CH_2)_n$	0.88(m)	P
8	VLDL	$CH_3CH_2CH_2C=$	0.89(m)	P
9	β-OH-isobutyrate	βCH_3, βCH_2	1.14(d), 3.73(dd)	P
10	β-OH-butyrate	γCH_3, βCH, αCH_2	1.2(d), 4.23(m), 2.31(dd), 2.38(dd)	P
11	lipid	$(CH_2)_n$, CH_2—C=C, =C—CH_2—C=, —CH=CH—	1.27(m), 2.03(m), 2.77(m), 5.30(m)	P
12	threonine	γCH_3, βCH_2, αCH	1.32(s), 4.28(m), 3.58(d)	P
13	lactate	βCH_3, αCH	1.33(d), 4.11(q)	P, U
14	alanine	βCH_3, αCH	1.48(d), 3.78(q)	P
15	lysine	γCH_2, δCH_2, βCH_2, εCH_2, αCH	1.47(m), 1.7(m), 1.89(m), 3.01(t), 3.78(t)	P, U
16	proline	βCH_2,γCH_2, βCH_2, δCH_2	2.07(m), 2.35(m), 3.38(m)	P
17	α-ketoadipate	αCH_2, βCH_2, γCH_2	2.77(t), 1.82(m), 2.22(t)	U
18	acetate	CH_3	1.91(s)	P, U
19	arginine	δCH_2, γCH_2, βCH_2, αCH	3.24(t), 1.68(m), 1.71(m), 1.91(m), 3.74(t)	U
20	*N*-acetyl-glycoprotein	CH_3	2.04(s)	P
21	*N*-acetyl-group	CH_3	2.05(s)	U
22	*O*-acetyl-glycoprotein	CH_3	2.14(s)	P
23	acetoacetate	CH_3	2.27(s)	P
24	glutamate	βCH_2, αCH	2.14(dd), 2.45(dd), 3.77(dd)	P
25	pyruvate	βCH_3	2.37(s)	P
26	succinate	CH_2	2.40(s)	U
27	2-oxoglutaric acid	βCH_2, γCH_2	3.02(t), 2.46(t)	U
28	citrate	half CH_2, half CH_2	2.53(d), 2.69(d)	P, U
29	DMA	CH_3	2.73(s)	U
30	TMA	CH_3	2.93(s)	U
31	creatine	CH_3, CH_2	3.04(s), 3.93(s)	P, U
32	asparate	half βCH_2, half βCH_2, αCH	2.67(dd), 2.81(dd), 3.88(dd)	P
33	choline	$N(CH_3)_3$	3.20(s)	P
34	TMAO	CH_3	3.26(s)	P
35	taurine	$-CH_2-S$, $-CH_2-NH_2$	3.28(t), 3.44(t)	U
36	betaine	CH_3, CH_2	3.23(s), 3.91(s)	U
37	creatinine	CH_3, CH_2	3.05(s), 4.06(s)	U
38	α-glucose	H1, H2, H3, H4, H5, H6, H6′	4.65(d), 3.24(dd), 3.49(t), 3.42(t), 3.47(m), 3.90(dd), 3.72(dd)	P, U
39	β-glucose	H1, H2, H3, H4, H5, H6, H6′	5.24(d), 3.53(dd), 3.69(t), 3.39(t), 3.81(m), 3.71(dd), 3.73(dd)	P, U
40	glycerophosphocholine	CH_3	3.22(s)	P
41	fumarate	CH	6.52(s)	P, U
42	*trans*-aconitate	=CH, CH_2	6.66(s), 3.45(s)	U
43	tyrosine	H3 & H5, H2 & H6	6.89(m), 7.18(m)	P, U
44	histidine	H4, H2	7.05(s), 7.75(s)	P
45	phenylalanine	H2 & H6, H4, H3 & H5	7.31(m), 7.37(m), 7.42(m)	P, U
46	benozate	H2 & H6, H3 & H5, H4	7.88(m), 7.49(m), 7.56(m)	U
47	hippurate	CH_2, NH, H2 & H6, H3 & H5, H4	3.97(d), 8.55(s), 7.84(d), 7.56(t), 7.65(t)	U
48	formate	H—COOH	8.45(s)	P, U
49	NAD^+	H3, H2	8.84(d), 9.13(d)	U
U1	unknown 1		3.15	P
U2	unknown 2		6.06(s)	U

[a]P: plasma; U: urine; Multiplicity: singlet (s), doublets (d), triplets (t), doublet of doublets (dd), multiplets (m); quartets (q).

RESULTS AND DISCUSSION

Clinical Chemistry and Histopathological Assessments of the Streptozotocin-Induced Rat Models

The random blood sugar (RBS) levels for most of the streptozotocin (STZ) treated rats reached 16.7 mM on day 4 postdose and remained at such high level on day 9, which met the diagnostic criteria of diabetes. However, four animals (T2, T4, T16, and T18) failed to develop diabetes with RBS below 7.0 mM at day 4 and day 9 (Figure S1A, Supporting Information (SI)). This implies that rat responses to STZ are heterogeneous, which is in good agreement with previous

dx.doi.org/10.1021/pr300280t | J. Proteome Res. 2012, 11, 3423−3435

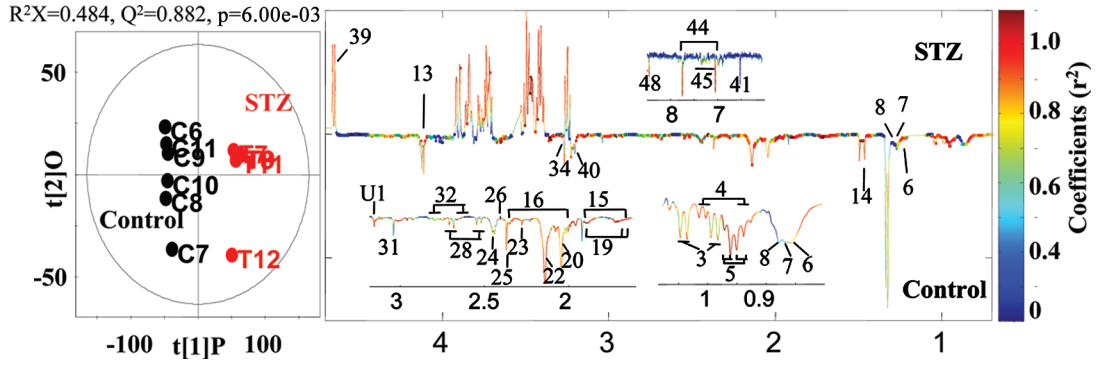

Figure 2. OPLS-DA results for controls and streptozotocin (STZ)-treated rats derived from ^{1}H NMR CPMG spectra of plasma. The keys for metabolites are given in Table 2.

findings.[50] In fact, such heterogeneous responses were also evident even when the STZ dosage was as high as 65 mg/kg (i.v.).[43]

Compared with controls, the hyperglycemia rats showed clear cellular edema, vacuolar degeneration, and reduction of cell population in their pancreas tissue (Figure S1B, SI). This implies that the successful models of STZ-diabetes in this study are based on selective destruction of pancreatic β-cells as well-established before and thus reach a state of absolute insulinopenia, which is similar to type 1 diabetes mellitus (T1DM) in humans. Clinical chemistry results showed that STZ treatment led to significant ALT increase (Figure S2, SI), indicating hepatic dysfunction, and significant decrease in ALB (Figure S2, SI), suggesting disruption of protein biosynthesis and probably disturbance in amino acid metabolism.

STZ-Induced Plasma Metabonomic Changes

Figure 1 shows ^{1}H NMR spectra of blood plasma of a control and STZ-treated rat on day 12 post-treatment. The spectral signals were assigned (Table 1) according to literature data[45,51] and public and in-house developed databases with further confirmation from a catalogue of 2D NMR spectra including COSY, TOCSY, JRES, HSQC, and HMBC 2D NMR spectra. Apart from the lipid signals, the spectra contained numerous resonances from other metabolites including glucose, branched-chain amino acids (valine, isoleucine, leucine), basic amino acids (lysine, arginine, histidine), acidic amino acids (glutamate, asparate), aromatic amino acids (tyrosine, phenylalanine), other aliphatic amino acids (alanine, threonine, proline), ketone bodies (β-OH-butyrate and acetoacetate), several carboxylic acids (β-OH-isobutyrate, acetate and formate), choline, TMAO, glycolysis and TCA intermediates (lactate and citrate). Visual inspection revealed obvious level differences for glucose between two groups, indicating that STZ induced alterations in glucose metabolism.

To obtain the detailed metabolic changes induced by STZ and metabolic pathways involved, we performed OPLS-DA with the nonresponders removed from the treated group. The scores plot from OPLS-DA (Figure 2) indicated significant metabonomic differences between control and STZ responders with good model quality (R^2X = 0.484, Q^2 = 0.882, p = 0.006). The corresponding loadings plot (Figure 2) showed that STZ treatment resulted in significant elevation of blood glucose but decline of gluconeogenesis precursors such as glutamine, aspartate, and alanine, glycolysis product (lactate), TCA cycle intermediate (citrate), branched-chain amino acids (BCAAs) (valine, leucine and isoleucine), some basic amino acids (histidine, lysine and arginine), formate, and TMAO. The altered metabolites and their corresponding correlation coefficients are tabulated in Table 2.

These observations indicated that STZ treatment induced marked depression of both aerobic and anaerobic glycolysis. This is also consistent with the fact that STZ causes absolute hypoinsulinemia, which further leads to a reduction of glucose uptake and an impairment of glucose utilization in peripheral tissues, such as skeletal muscles and adipose tissue.[52] Since lactate, alanine, valine, isoleucine, and asparagine are important precursors of gluconeogenesis in liver and kidney, their level decreases probably also reflect STZ-induced promotion of gluconeogenesis, which is consistent with what is observed for T1DM.[53] Our results showed that the levels of all branched-chain amino acids (BCAAs) were decreased by STZ treatment. Although the changes of BCAAs were not consistent with the observations for prolonged diabetic effects, the observation here may reflect the BCAA changes at early stage of T1DM development and probably implies that, with inhibition of glycolysis, BCAAs may have been fed into TCA cycle to produce adenosine triphosphate (ATP) in skeletal muscle.[54] BCAAs reduction may also be related to promotion of gluconeogenesis, which will inevitably reduce the levels of glucogenic amino acids such as alanine, valine, and isoleucine.

The concentration decrease of histidine in plasma observed in STZ-induced group is consistent with the STZ-induced activity enhancement for histidine decarboxylase.[55] Such is probably related to metabolism of histamine since it is well-known that histamine mediates alterations in microvessel and macrovessel endothelial permeability contributing to the pathogenesis of initial damage in atherosclerosis.[55,56] Our observation of the level decrease for histidine probably implies increased histamine biosynthesis and may be an early sign for the occurrence of T1DM complications.

Such a notion is supported with the STZ-induced decrease of plasma lysine, which is probably related to activation of oxidative deamination mediated by the reactive oxygen species (ROS).[57] Under such circumstances, lysine is transformed into allysine, which is a precursor for the formation of advanced glycosylation end-products (AGEs) in diabetes.[57,58] Therefore, such changes in lysine may also imply the early development of diabetic complications at the molecular level.[58] This is further reflected in the STZ-induced decrease of plasma arginine, probably indicating the involvement of nitric oxide (NO) pathway since arginine is the precursor of NO produced via NO synthase (NOS) catalysis and functioning for the maintenance of vascular homeostasis. Furthermore, the reduction of arginine level may also be related to the biosynthesis of

Table 2. Coefficients for Plasma Metabolites Significantly Contributed to Differentiations between the Control and STZ-Induced Diabetic Rats

metabolites	δ ^{1}H (ppm)	coefficient value[a]
isoleucine	0.930, 1.003	−0.95
leucine	0.945, 0.960	−0.94
valine	0.982, 1.030	−0.82
alanine	1.465, 1.495	−0.90
glucose	5.235	+0.93
pyruvate	2.371	−0.84
lactate	4.111	−0.86
citrate	2.547, 2.684	−0.96
acetoacetate	2.271	−0.86
asparate	2.640, 2.813	−0.87
glutamate	2.450	−0.84
lysine	1.711, 1.894, 3.011	−0.97
histidine	7.051, 7.751	−0.95
arginine	1.681, 1.712, 1.911	−0.92
tyrosine	7.162	−0.84
phenylalaine	7.312, 7.363, 7.409	−0.83
proline	2.351, 2.071	−0.89
N-acetyl-glycoprotein	2.041	−0.84
O-acetyl-glycoprotein	2.141	−0.90
GPC	3.229	−0.81
HDL	0.848, 1.241	−0.87
formate	8.458	−0.93
TMAO	3.268	−0.86

[a]The + and − signs indicate metabolite concentration increase and decrease respectively for diabetic rats compared with normal rats ($p < 0.05$). GPC: glycerophosphocholine.

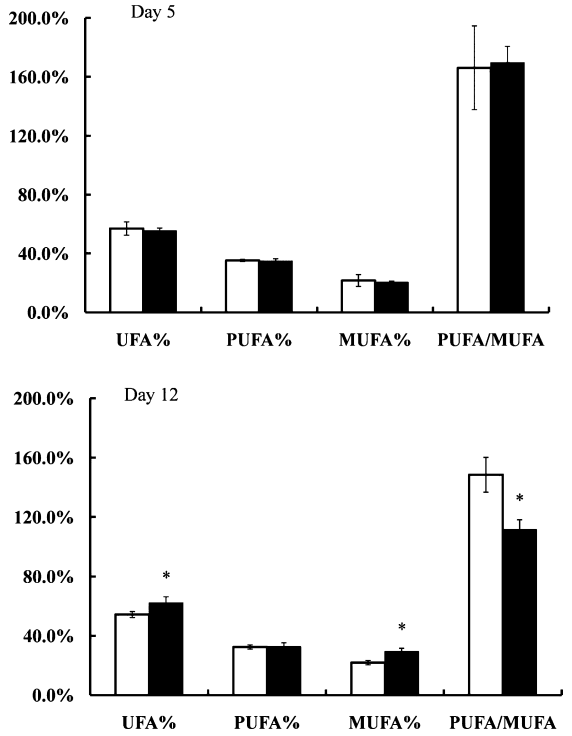

Figure 3. Data for unsaturated fatty acid (UFA), polyunsaturated fatty acid (PUFA), monounsaturated fatty acid (MUFA), and PUFA-to-MUFA ratio derived from diffusion-edited ^{1}H NMR spectra of plasma for controls (white bar) and streptozotocin (STZ)-treated rats (black bar) on day 12 postdose. * $p < 0.05$ when compared to controls.

asymmetric dimethylarginine (ADMA). Since ADMA can impair NO production by competitive inhibition of NOS, it has been considered as an independent risk marker for cardiovascular disease.[59] In fact, previous work has already found the association between declined plasma arginine and elevated ADMA in type 1 diabetic subjects without apparent vascular complications.[60] STZ-induced significant decrease of albumin (ALB) in rat plasma (Figure S2, SI) is probably associated with the STZ-caused secretion dysfunction of insulin. Such dysfunction inevitably causes increased protein catabolism, and the produced amino acids can then be utilized as precursors for gluconeogenesis and/or ATP generation through oxidation and TCA cycle.

STZ treatment resulted in significant dyslipidemia including both lipoproteins and fatty acids. The STZ-induced diabetic rats showed lower HDL levels, being consistent with low HDL-cholesterol concentrations observed for diabetes.[61] LDL did not show significant changes in the STZ-group, which also agreed well with the previous results for diabetes, especially at the early stages.[61]

Moreover, we further found (Figure 3) that at day 12 after STZ-treatment, significant alterations were observable in the blood plasma contents of unsaturated fatty acids (UFA). The contents of both UFA and MUFA were significantly increased, whereas the PUFA-to-MUFA ratio was significantly reduced in the STZ-group compared with controls. Such changes were not observed at day 5 after STZ treatment (Figure 3). Literature searches have revealed that such observations have not yet been reported previously. The reduction of PUFA-to-MUFA ratio (Figure 3) is probably related to STZ-induced oxidative stress and represents a surrogate marker for lipid per-oxidation. Such peroxidation process is normally initiated with free radical reactions, and the resultant reactive oxygen species causes NMR signal losses for CH_2 moieties (δ 2.70−2.85) situated between two double bonds in PUFA, leading to damages to cell membranes subsequently.

The above findings, therefore, suggested that STZ-induced insulinopenia caused comprehensive metabolic changes including depression of glycolysis and promotion of gluconeogenesis, enhanced oxidative stresses, alterations in basic amino acids associated with diabetic complications and dysfunction in energy metabolisms. STZ-induced level reductions for TMAO and formate may be related to alterations to choline metabolism and/or perhaps changes in gut microbiota functions, which ought to be highlighted in the STZ-induced urinary metabonomic changes as well.

Dynamic Metabonomic Changes in Rat Urines Associated with the Progression of STZ-Induced Diabetes

^{1}H NMR spectra (Figure S3, SI) showed that the detected endogenous metabolites in the urine samples from the STZ-induced diabetic rats included short-chain fatty acids (formate, acetate, and butyrate), keto acids (α-keto-β-methyl-*N*-valerate, and α-ketoadipate), TCA cycle intermediates (succinate, 2-oxoglutarate, citrate, and fumarate), amino acids (alanine, lysine, tyrosine, and phenylalanine), creatine, creatinine, and gut microbiota-related metabolites (DMA, TMA, benzoate, and hippurate). After day 2 postdose, the drastically elevated levels for urinary glucose and lactate can be easily observed for the STZ-treated rats (Figure S3, SI).

PCA metabolic trajectory plots constructed from the NMR data at four typical time points (Figure S4A, SI) showed overall dynamic changes of rat metabonome. These four time points

dx.doi.org/10.1021/pr300280t | J. Proteome Res. 2012, 11, 3423−3435

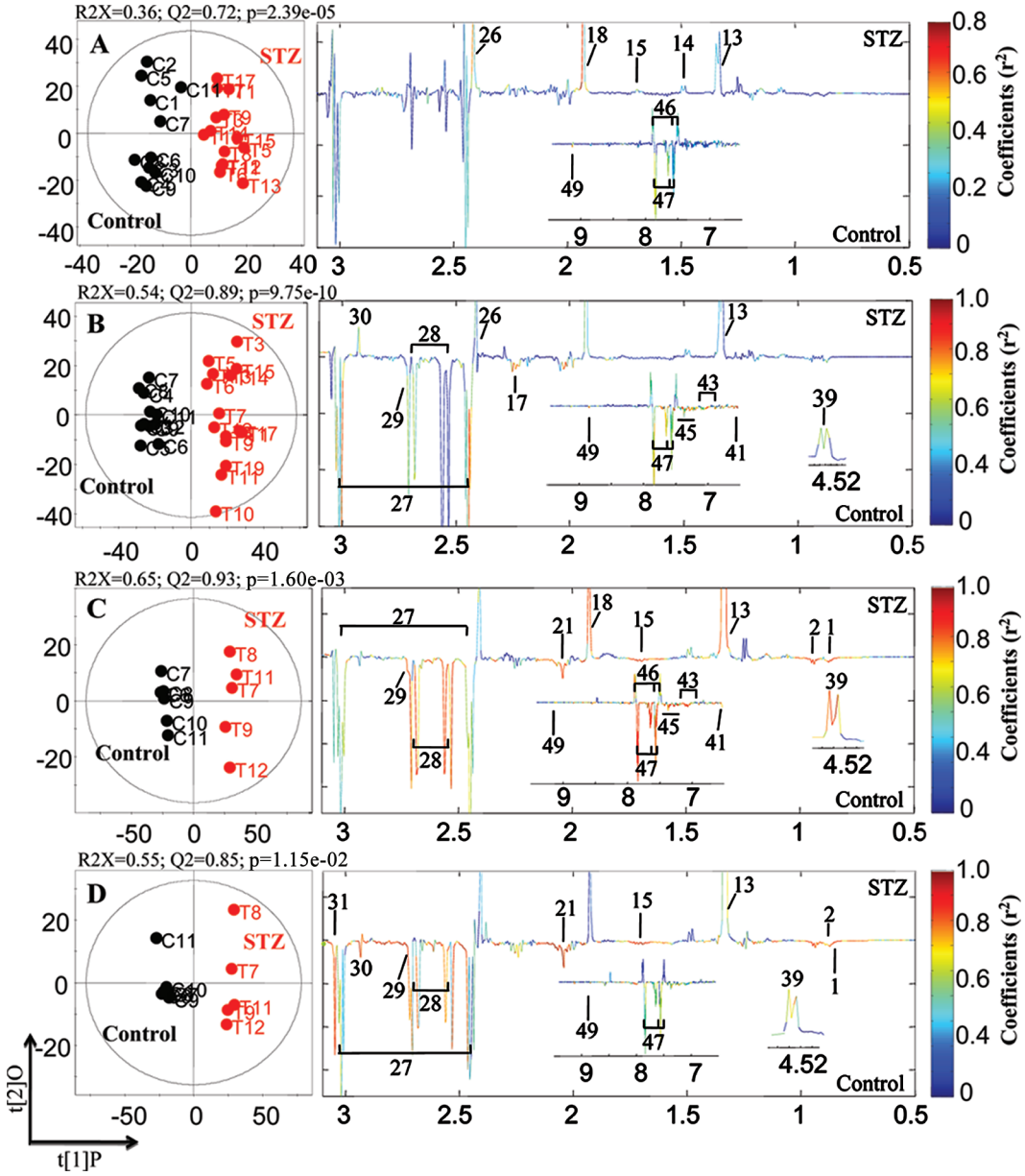

Figure 4. OPLS-DA results for controls and streptozotocin (STZ)-treated rats derived from ^{1}H NMR spectra of urine sampels on day 1 (A), day 2 (B), day 4 (C), and day 11 (D) postdose excluding the STZ nonresponders. The keys for metabolites are given in Table 3.

included predose and days 1, 2, 4, and 11 postdose (Figure S4A, SI), with data for days 4−11 largely clustered together (data not shown). The results (Figure S4A, SI) showed that an obvious difference was observable between urinary metabolic profiles for controls and STZ-treated groups from day 2 postdose, whereas the changes of metabolic profiles appeared to have reached a steady state after day 4. Importantly, PCA results also indicated some metabonomic differences between controls and STZ-treated rats as early as day 1 postdose (Figure S4B, SI), even though neither glucosuria nor obvious relevant symptoms of diabetes, such as polydipsia and polyuria, were observable for the STZ-treated rats. Therefore, the changes observed on day 1 postdose were initial state of the rat responses to streptozotocin administration. These observations are significantly important since this STZ-induced diabetes is well regarded to be the mimic of type 1 diabetes in human in terms of dysfunctions of pancreatic β-cells and absolute insulinopenia, and our observations are probably relevant to the "initiation stage" of type 1 diabetes.

To extract detailed information on the STZ-induced metabolic changes at this early stage of diabetes, OPLS-DA was performed on the rat urinary metabolic profiles of the STZ-treated and time-matched control groups on the day 1 postdose. The results showed that compared with controls, STZ treatment caused significant elevation of urinary lactate, alanine, succinate, acetate, and lysine and level reductions for NAD^+, hippurate, and tyrosine (Figure 4). These early rat metabolic responses to STZ treatment seemed to include the alterations in TCA cycle and gut microbiota functions. Elevation of amino acids such as alanine and lysine may indicate STZ-induced renal glomerular filtration deficiency and thus stresses to kidney functions, whereas decline of NAD^+ is probably associated with oxidative stress under the status of diabetes.[62] The above results also suggest that metabonomic analysis is effective to obtain the information on the

dx.doi.org/10.1021/pr300280t | J. Proteome Res. 2012, 11, 3423−3435

Table 3. Coefficients for Urinary Metabolites Significantly Contributed to Differentiations between the Streptozotocin (STZ)-Treated and Control Rats[a]

Metabolites	Coefficients										
	Day01[b]	Day02	Day03	Day04	Day05	Day06	Day07	Day08	Day09	Day10	Day11
α-keto-β-methyl-N-valerate		-0.817	-0.895	-0.707	-0.922	-0.908	-0.919		-0.905	-0.887	-0.959
butyrate		-0.646	-0.932	-0.695	-0.939	-0.888	-0.897	-0.892	-0.883	-0.916	-0.966
lactate	+0.581	+0.775	+0.831	+0.797	+0.933	+0.873	+0.973	+0.864	+0.815	+0.883	+0.951
alanine	+0.607		+0.798	+0.739							
lysine	+0.665		-0.844	-0.718	-0.912	-0.834	-0.856	-0.855	-0.874	-0.941	-0.866
α-ketoadipate		-0.661	-0.868								-0.848
acetate	+0.742	+0.626	+0.771	+0.754	+0.941						+0.934
α-ketoadipate		-0.924	-0.716	-0.819		-0.864					-0.858
succinate	+0.655	+0.694	+0.605	+0.607							
citrate		-0.577	-0.825	-0.850	-0.926	-0.926	-0.890	-0.879		-0.845	-0.822
DMA		-0.767		-0.691	-0.885						-0.920
TMA		+0.717	+0.671	+0.756							
2-oxoglutarate		-0.741	-0.860	-0.764		-0.827		-0.957			-0.835
creatine			-0.890		-0.867	-0.909		-0.887	-0.871	-0.940	-0.818
hippurate	-0.679	-0.891	-0.910	-0.820	-0.923		-0.865				-0.912
creatinine			-0.938	-0.636	-0.825	-0.903		-0.866	-0.865	-0.933	-0.856
glucose		+0.856	+0.917	+0.883	+0.946	+0.971	+0.884	+0.853	+0.988	+0.831	+0.983
allantion			-0.938								
fumarate		-0.837	-0.937	-0.919	-0.820						-0.888
trans-aconitate			-0.746	-0.646							
tyrosine	-0.678	-0.761	-0.950	-0.875	-0.940		-0.919				-0.904
phenylalanine		-0.847	-0.941		-0.953				-0.852		-0.871
benzoate		+0.623	+0.904	+0.823	+0.864						+0.917
formate			+0.698								+0.852
NAD+	-0.602	-0.788	-0.887	-0.733			-0.823		-0.889	-0.883	

[a]The + and − signs indicate metabolite level increase and decrease respectively for diabetic rats compared with controls at the level of $p < 0.05$. [b]Day 1 postdose.

disease-caused endogenous perturbations at the early onset stages, even prior to the occurrence of hyperglycemia.

Such impairment will inevitably result in changes in glycolysis/gluconeogenesis and disturbance to TCA cycle (Table 3). This is reflected in the level changes of TCA cycle intermediates including the level elevation for succinate and decline for fumarate, 2-OG, and citrate after day 2 postdose. In fact, such level changes for succinate and fumarate further indicate the decrease of succinate dehydrogenase activities (SDH), which has been observed in skeletal muscles under insulinopenia.[63] The decrease of 2-OG is consistent with the STZ-induced enhancement of the 2-OG carboxylase activities in rat liver mitochondria and agrees with enhanced gluconeogenesis in the STZ-induced type 1 diabetes.[64] The STZ-induced level changes for amino acids suggest that they are used as energy sources to compensate the energy shortages due to depressed utilization of glucose. Such is confirmable by the significant level decreases of α-keto-β-methyl-*N*-valerate and α-ketoadipate, which are the oxidative metabolites of isoleucine and lysine, respectively. These keto-acids can then be transformed into acetyl-CoA and subsequently consumed in TCA cycle for production of adenosine triphosphate (ATP).

Urinary creatinine had significant level decrease upon a single STZ injection. As a breakdown product of creatine phosphate in muscles, creatinine is normally eliminated from kidneys by the glomerular filtration with partial tubular excretion. Under normal circumstances, urinary creatinine level is fairly constant. The decline of urinary creatinine might also be related to the decrease of muscle mass since in this study we actually observed the decreases in body weights for the diabetic rats (Figure S5, SI). Such an observation further indicates that care has to be taken when using the creatinine concentration to normalize urinalysis for clinical chemistry and metabonomics studies.

OPLS-DA results for the STZ-group and the time-matched controls (Figure 4) revealed substantially altered metabolites and their coefficients (Table 3) reflecting the dynamic changes of urinary metabonome associated with diabetes progression. The significance of the changes for these metabolites was color-coded ($p < 0.05$, in Table 3), with red color showing STZ-induced elevation and blue indicating level decline due to STZ administration. In these analyses, all the nonresponders were excluded from the modeling. All glucose signals were also removed prior to data normalization since the urine samples of the STZ-group contained much higher glucose levels (>20 times) than controls (Figure S4C, SI), as reported previously.[41] Although such practice will inevitably remove some overlapped signals mostly from α-protons of amino acids, this will not affect observation of the changes for amino acids since most of them have other signals located outside the discarded region. It has to be pointed that all signals for a few metabolites will be lost with the above practice, such as *myo*-inositol, taurine, and glycine. Nevertheless, the results obtained here will also be conserved and thus safe.

Nevertheless, drastic elevation of urinary glucose was still clearly observable during days 2−11 postdose from the ^{13}C satellite signals of the glucose anomeric proton, i.e., the doublet at 4.52 ppm (Figure 4). This was also clearly illustrated in the rate of changes for urinary glucose (Figure S4C, SI). Such is probably related to the STZ-induced specific destruction to pancreatic β-cells and thus the insulin secretion dysfunction.[43,65] It is well-known that, under normal physiological conditions, there is a functional balance between insulin and its counter-regulatory

dx.doi.org/10.1021/pr300280t | J. Proteome Res. 2012, 11, 3423−3435

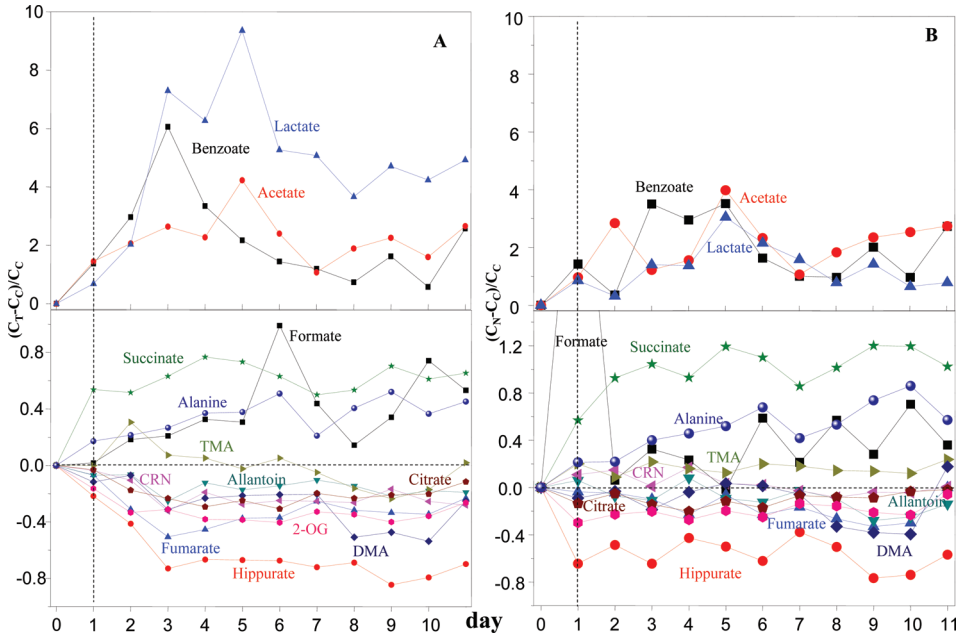

Figure 5. Ratios of dynamic changes for the urinary metabolite concentrations for the streptozotocin (STZ)-treated rats (A) and nonresponders (B) relative to controls. CRN: creatinine.

hormones such as glucagon, growth hormone, catecholamine, and glucocorticoid. With STZ-induced insulinopenia, such balance is overwhelmingly reversed, and insulin can no longer perform its due functions[38] while the counter-regulatory hormones predominate. Consequently, an absolute reduction of glucose uptake, especially in skeletal muscles and adipose tissues, will occur accompanied with an impairment of glucose utilization as energy source.

Furthermore, STZ injection led to level changes for metabolites probably associated with the gut microbiota, highlighted with the lower level for hippurate accompanied with higher level for benzoate in diabetic rats. The level decline of urinary benzoate was not reported or discussed for STZ-induced diabetes rats in previous studies. However, close inspection of the NMR spectra reported previously[41] revealed that this metabolite was visible there. Benzoate is a known byproduct of phenylalanine metabolism of bacteria, which is normally conjugated with glycine in the mammalian liver and excreted as urinary hippurate.[66] Therefore, STZ-induced dysfunction of liver glycine conjugation seems to be inferred here as well. The STZ-induced elevation of TMA and decline of DMA in diabetic rat urine further support the notion that gut microbiota are probably involved in development of diabetes since these organic amines are bacterial metabolites from choline. It is likely that the changes of short-chain fatty acids (SCFAs) such as acetate and butyrate may also be associated with the changes to gut microbiota since these SCFAs are normally produced through gut bacterial fermentation of complex carbohydrates such as cellulose and resistant starches.[67,68] However, the precise roles of gut microbiota in development and progression of diabetes remain to be investigated with functional metagenomics approaches.

To characterize the dynamic changes of metabolites caused by STZ administration, the resonances of metabolites having the least overlap with others were chosen to calculate their changes relative to control group for each day. The results showed that STZ-induced dynamic changes were observable for a number of urinary metabolites (Figure 5A). Urinary glucose signals were barely detectable in the predose and control samples (Figure S4C, SI). However, these signals were drastically elevated in the STZ-treated rat urine samples from day 2 postdose (Figure S4C, SI) and remained in high level (about 20 times compared to control group) on day 11 postdose (Figure S4C, SI). On day 2 postdose, some other metabolites also showed obvious level changes (Figure 5A) including TCA cycle intermediates (2-oxoglutarate, citrate, and fumarate) and metabolites related to the gut microbiota (TMA and benzoate). Even on day 1 postdose, some STZ-induced changes (Figure 5A) were clearly visible including glycolysis-related metabolites (lactate), TCA cycle intermediates (succinate), and gut microbiota-related metabolites (benzoate and hippurate).

The results showed that lactate had the most outstanding changes (apart from glucose) with maximum level observed on day 3 postdose (about 10-fold increase). After that, it maintained high level for the following two days and showed a gradual decrease to about 4-fold level compared to controls after day 7 postdose (Figure 5A). Acetate levels had similar trend though limited to a narrower range. Benzoate in STZ-treated rat urine samples reached about 6-fold higher level than that in controls on the day 3 postdose and maintained around 1-fold higher than controls after day 7 postdose (Figure 5A). To the best of our knowledge, this has not been reported previously. Other metabolites also showed time-dependent changes though to a lesser degree. Succinate in TCA cycle showed about 60% STZ-induced increase, while fumarate had 30−60% decrease, indicating the change of SDH activity. Gut microbiota related metabolites, hippurate and DMA, also showed about 40 and 80% decrease, respectively, relative to controls for days 2−11 post-STZ-treatment (Figure 5A).

Apparent heterogeneity is present in terms of metabolic responses to the STZ-treatments. Four rats (T2, T4, T16, and T18) failed to show hyperglycemia upon STZ treatment (Figure S1A, SI), and their metabonomic features seemed to be more similar to controls (Figure S4C, SI). Such STZ resistance was mentioned in previous studies[50] where metabolites related

dx.doi.org/10.1021/pr300280t | J. Proteome Res. 2012, 11, 3423−3435

to gut microbiota were implicated,[50] even though such was not mentioned in another previous study for the STZ-treated female rats.[41] However, unlike reported results, our analysis on both the urinary and fecal metabolite composition prior to STZ treatment did not show significant differences between these nonresponders and responders. No outstanding differences in metabolite changes (relative to controls) were observed (Figure 5B) between the STZ-treated responders and non-responders for microbiota-related metabolites such as hippurate and benzoate. In fact, these nonresponders also showed STZ-induced elevations for acetate, lactate, succinate, and alanine together with decreases of fumarate though to a different extent (Figure 5B). This probably implies that STZ can also cause similar changes in TCA cycle for nonresponders as well. Therefore, one can speculate that this nonresponse to STZ may be related to lower GLUT2 activity in pancreatic β-cells with ATP-sensitive K^+ channel (K_{ATP} channel)-deficiency as reported previously.[69]

It was striking to notice that urinary glucose of one STZ-treated rat (T10) had obvious elevation on day 2 (Figure S4C, SI) but returned to normal level on day 9 postdose. Such recovery has not been reported to the best of our knowledge, further supporting the notion of STZ-response heterogeneity for rats. It is difficult to ascertain the underlying mechanism with only 1 out of 19 rats showing such recovery. However, this may be related to regeneration of pancreatic islet cells with a transient hyperglycemia observed within 48 h following a single dose of STZ (70 mg/kg) on the neonatal rat.[70] In such case, blood glucose returned to normality within 2 weeks, and small clusters of highly proliferative β-cells were observable near ducts.[70] The exact reasons for such self-recovery of the streptozotocin-induced diabetes model warrant further investigation.

CONCLUSIONS

This study showed that metabolic responses of rats to STZ-treatment with a moderate dosage were systematic involving changes in glycolysis/gluconeogenesis, lipid metabolism, oxidation of amino acids, TCA cycle, choline metabolism, liver conjugations, and gut microbiota functions. Such responses are dynamic with time-dependence. STZ-treatment induced significant level rise of total unsaturated fatty acids and monounsaturated fatty acids in blood plasma accompanied with reduction of PUFA-to-MUFA ratio. Even before hyperglycemia was developed, STZ-induced metabonomic changes were already observable in urinary metabolic profiles. The rat responses to STZ-treatment were heterogeneous, with some rats showing resistance and a single rat showing a positive response but complete recovery as well. These results have indicated that metabonomic analysis of urine and blood plasma is potentially important to monitor the dynamic changes associated with metabolic disorders with the possibility to detect diseases in the early stages.

ASSOCIATED CONTENT

Supporting Information

Supplementary Figures S1–S5. This material is available free of charge via the Internet at http://pubs.acs.org.

AUTHOR INFORMATION

Corresponding Author

*Tel.: +86-(0)27-87198430. Fax: +86-(0)27-87199291. E-mail: huiru.tang@wipm.ac.cn.

Notes

The authors declare no competing financial interest.

ACKNOWLEDGMENTS

We acknowledge financial support from the National Basic Research Program of China (2009CB118804, 2010CB912501, and 2007CB914701), the National Natural Science Foundation of China (20825520, 20775087, 20775086, and 21175149), and the Chinese Academy of Sciences (KJCX2-YW-W11, KSCX1-YW-02).

REFERENCES

(1) Roglic, G.; Unwin, N.; Bennett, P. H.; Mathers, C.; Tuomilehto, J.; Nag, S.; Connolly, V.; King, H. The burden of mortality attributable to diabetes: realistic estimates for the year 2000. *Diabetes Care* **2005**, *28* (9), 2130–2135.

(2) American Diabetes Association. Diagnosis and classification of diabetes mellitus. *Diabetes Care* **2004**, *27* (1 Suppl), S5–S10.

(3) Wild, S.; Roglic, G.; Green, A.; Sicree, R.; King, H. Global prevalence of diabetes: estimates for the year 2000 and projections for 2030. *Diabetes Care* **2004**, *27* (5), 1047–1053.

(4) Nathan, D. M.; Cleary, P. A.; Backlund, J. Y.; Genuth, S. M.; Lachin, J. M.; Orchard, T. J.; Raskin, P.; Zinman, B. Intensive diabetes treatment and cardiovascular disease in patients with type 1 diabetes. *N. Engl. J. Med.* **2005**, *353* (25), 2643–2653.

(5) Holman, R. R.; Paul, S. K.; Bethel, M. A.; Matthews, D. R.; Neil, H. A. 10-year follow-up of intensive glucose control in type 2 diabetes. *N. Engl. J. Med.* **2008**, *359* (15), 1577–1589.

(6) Patel, A.; MacMahon, S.; Chalmers, J.; Neal, B.; Billot, L.; Woodward, M.; Marre, M.; Cooper, M.; Glasziou, P.; Grobbee, D.; Hamet, P.; Harrap, S.; Heller, S.; Liu, L.; Mancia, G.; Mogensen, C. E.; Pan, C.; Poulter, N.; Rodgers, A.; Williams, B.; Bompoint, S.; de Galan, B. E.; Joshi, R.; Travert, F. Intensive blood glucose control and vascular outcomes in patients with type 2 diabetes. *N. Engl. J. Med.* **2008**, *358* (24), 2560–2572.

(7) Gerstein, H. C.; Miller, M. E.; Byington, R. P.; Goff, D. C. J.; Bigger, J. T.; Buse, J. B.; Cushman, W. C.; Genuth, S.; Ismail-Beigi, F.; Grimm, R. H. J.; Probstfield, J. L.; Simons-Morton, D. G.; Friedewald, W. T. Effects of intensive glucose lowering in type 2 diabetes. *N. Engl. J. Med.* **2008**, *358* (24), 2545–2559.

(8) American Diabetes Association. Standards of medical care in diabetes—2011. *Diabetes Care* **2011**, *34* (Suppl 1), S11–S61.

(9) Maier, L. M.; Wicker, L. S. Genetic susceptibility to type 1 diabetes. *Curr. Opin. Immunol.* **2005**, *17* (6), 601–608.

(10) Thomson, G.; Valdes, A. M.; Noble, J. A.; Kockum, I.; Grote, M. N.; Najman, J.; Erlich, H. A.; Cucca, F.; Pugliese, A.; Steenkiste, A.; Dorman, J. S.; Caillat-Zucman, S.; Hermann, R.; Ilonen, J.; Lambert, A. P.; Bingley, P. J.; Gillespie, K. M.; Lernmark, A.; Sanjeevi, C. B.; Ronningen, K. S.; Undlien, D. E.; Thorsby, E.; Petrone, A.; Buzzetti, R.; Koeleman, B. P.; Roep, B. O.; Saruhan-Direskeneli, G.; Uyar, F. A.; Gunoz, H.; Gorodezky, C.; Alaez, C.; Boehm, B. O.; Mlynarski, W.; Ikegami, H.; Berrino, M.; Fasano, M. E.; Dametto, E.; Israel, S.; Brautbar, C.; Santiago-Cortes, A.; Frazer de Llado, T.; She, J. X.; Bugawan, T. L.; Rotter, J. I.; Raffel, L.; Zeidler, A.; Leyva-Cobian, F.; Hawkins, B. R.; Chan, S. H.; Castano, L.; Pociot, F.; Nerup, J. Relative predispositional effects of HLA class II DRB1-DQB1 haplotypes and genotypes on type 1 diabetes: a meta-analysis. *Tissue Antigens* **2007**, *70* (2), 110–127.

(11) Todd, J. A.; Bell, J. I.; McDevitt, H. O. HLA-DQ beta gene contributes to susceptibility and resistance to insulin-dependent diabetes mellitus. *Nature* **1987**, *329* (6140), 599–604.

(12) Barratt, B. J.; Payne, F.; Lowe, C. E.; Hermann, R.; Healy, B. C.; Harold, D.; Concannon, P.; Gharani, N.; McCarthy, M. I.; Olavesen, M. G.; McCormack, R.; Guja, C.; Ionescu-Tirgoviste, C.; Undlien, D. E.; Ronningen, K. S.; Gillespie, K. M.; Tuomilehto-Wolf, E.; Tuomilehto, J.; Bennett, S. T.; Clayton, D. G.; Cordell, H. J.; Todd, J. A.

Remapping the insulin gene/IDDM2 locus in type 1 diabetes. *Diabetes* **2004**, *53* (7), 1884−1889.
(13) Marron, M. P.; Raffel, L. J.; Garchon, H. J.; Jacob, C. O.; Serrano-Rios, M.; Martinez Larrad, M. T.; Teng, W. P.; Park, Y.; Zhang, Z. X.; Goldstein, D. R.; Tao, Y. W.; Beaurain, G.; Bach, J. F.; Huang, H. S.; Luo, D. F.; Zeidler, A.; Rotter, J. I.; Yang, M. C.; Modilevsky, T.; Maclaren, N. K.; She, J. X. Insulin-dependent diabetes mellitus (IDDM) is associated with CTLA4 polymorphisms in multiple ethnic groups. *Hum. Mol. Genet.* **1997**, *6* (8), 1275−1282.
(14) Mandrup-Poulsen, T. The role of interleukin-1 in the pathogenesis of IDDM. *Diabetologia* **1996**, *39* (9), 1005−1029.
(15) Larsen, P. M.; Fey, S. J.; Larsen, M. R.; Nawrocki, A.; Andersen, H. U.; Kahler, H.; Heilmann, C.; Voss, M. C.; Roepstorff, P.; Pociot, F.; Karlsen, A. E.; Nerup, J. Proteome analysis of interleukin-1beta—induced changes in protein expression in rat islets of Langerhans. *Diabetes* **2001**, *50* (5), 1056−1063.
(16) Lyssenko, V.; Jonsson, A.; Almgren, P.; Pulizzi, N.; Isomaa, B.; Tuomi, T.; Berglund, G.; Altshuler, D.; Nilsson, P.; Groop, L. Clinical risk factors, DNA variants, and the development of type 2 diabetes. *N. Engl. J. Med.* **2008**, *359* (21), 2220−2232.
(17) Lu, H.; Yang, Y.; Allister, E. M.; Wijesekara, N.; Wheeler, M. B. The identification of potential factors associated with the development of type 2 diabetes: a quantitative proteomics approach. *Mol. Cell. Proteomics* **2008**, *7* (8), 1434−1451.
(18) Tang, H. R.; Wang, Y. L. Metabonomics: a revolution in progress. *Prog. Biophys. Biochem.* **2006**, *33* (5), 401−417.
(19) Nicholson, J. K.; Wilson, I. D. Opinion: understanding "global" systems biology: metabonomics and the continuum of metabolism. *Nat. Rev. Drug Discovery* **2003**, *2* (8), 668−676.
(20) Nicholson, J. K.; Connelly, J.; Lindon, J. C.; Holmes, E. Metabonomics: a platform for studying drug toxicity and gene function. *Nat. Rev. Drug Discovery* **2002**, *1* (2), 153−161.
(21) Nicholson, J. K.; Lindon, J. C.; Holmes, E. "Metabonomics": understanding the metabolic responses of living systems to pathophysiological stimuli via multivariate statistical analysis of biological NMR spectroscopic data. *Xenobiotica* **1999**, *29* (11), 1181−1189.
(22) Griffin, J. L. Metabonomics: NMR spectroscopy and pattern recognition analysis of body fluids and tissues for characterisation of xenobiotic toxicity and disease diagnosis. *Curr. Opin. Chem. Biol.* **2003**, *7* (5), 648−654.
(23) Lindon, J. C.; Holmes, E.; Nicholson, J. K. Pattern recognition methods and applications in biomedical magnetic resonance. *Prog. Nucl. Magn. Reson. Spectrosc.* **2001**, *39* (1), 1−40.
(24) Teague, C.; Holmes, E.; Maibaum, E.; Nicholson, J.; Tang, H.; Chan, Q.; Elliott, P.; Stamler, J.; Ueshima, H.; Zhou, B.; Wilson, I. Ethyl glucoside in human urine following dietary exposure: detection by ^{1}H NMR spectroscopy as a result of metabonomic screening of humans. *Analyst* **2004**, *129* (3), 259−264.
(25) Wang, Y.; Holmes, E.; Tang, H.; Lindon, J. C.; Sprenger, N.; Turini, M. E.; Bergonzelli, G.; Fay, L. B.; Kochhar, S.; Nicholson, J. K. Experimental metabonomic model of dietary variation and stress interactions. *J. Proteome Res.* **2006**, *5* (7), 1535−1542.
(26) Yang, Y.; Li, C.; Nie, X.; Feng, X.; Chen, W.; Yue, Y.; Tang, H.; Deng, F. Metabonomic studies of human hepatocellular carcinoma using high-resolution magic-angle spinning ^{1}H NMR spectroscopy in conjunction with multivariate data analysis. *J. Proteome Res.* **2007**, *6* (7), 2605−2614.
(27) Yap, I. K.; Clayton, T. A.; Tang, H.; Everett, J. R.; Hanton, G.; Provost, J. P.; Le Net, J. L.; Charuel, C.; Lindon, J. C.; Nicholson, J. K. An integrated metabonomic approach to describe temporal metabolic disregulation induced in the rat by the model hepatotoxin allyl formate. *J. Proteome Res.* **2006**, *5* (10), 2675−2684.
(28) Bundy, J. G.; Lenz, E. M.; Bailey, N. J.; Gavaghan, C. L.; Svendsen, C.; Spurgeon, D.; Hankard, P. K.; Osborn, D.; Weeks, J. M.; Trauger, S. A.; Speir, P.; Sanders, I.; Lindon, J. C.; Nicholson, J. K.; Tang, H. Metabonomic assessment of toxicity of 4-fluoroaniline, 3,5-difluoroaniline and 2-fluoro-4-methylaniline to the earthworm Eisenia veneta (rosa): Identification of new endogenous biomarkers. *Environ. Toxicol. Chem.* **2002**, *21* (9), 1966−1972.
(29) Nicholson, J. K.; O'Flynn, M. P.; Sadler, P. J.; Macleod, A. F.; Juul, S. M.; Sonksen, P. H. Proton-nuclear-magnetic-resonance studies of serum, plasma and urine from fasting normal and diabetic subjects. *Biochem. J.* **1984**, *217* (2), 365−375.
(30) Wang, C.; Kong, H. W.; Guan, Y. F.; Yang, J.; Gu, J. R.; Yang, S. L.; Xu, G. W. Plasma phospholipid metabolic profiling and biomarkers of type 2 diabetes mellitus based on high-performance liquid chromatography/electrospray mass spectrometry and multivariate statistical analysis. *Anal. Chem.* **2005**, *77* (13), 4108−4116.
(31) Dumas, M. E.; Barton, R. H.; Toye, A.; Cloarec, O.; Blancher, C.; Rothwell, A.; Fearnside, J.; Tatoud, R.; Blanc, V.; Lindon, J. C.; Mitchell, S. C.; Holmes, E.; McCarthy, M. I.; Scott, J.; Gauguier, D.; Nicholson, J. K. Metabolic profiling reveals a contribution of gut microbiota to fatty liver phenotype in insulin-resistant mice. *Proc. Natl. Acad. Sci. U. S. A.* **2006**, *103* (33), 12511−12516.
(32) Li, M.; Wang, B. H.; Zhang, M. H.; Rantalainen, M.; Wang, S. Y.; Zhou, H. K.; Zhang, Y.; Shen, J.; Pang, X. Y.; Zhang, M. L.; Wei, H.; Chen, Y.; Lu, H. F.; Zuo, J.; Su, M. M.; Qiu, Y. P.; Jia, W.; Xiao, C. N.; Smith, L. M.; Yang, S. L.; Holmes, E.; Tang, H. R.; Zhao, G. P.; Nicholson, J. K.; Li, L. J.; Zhao, L. P. Symbiotic gut microbes modulate human metabolic phenotypes. *Proc. Natl. Acad. Sci. U. S. A.* **2008**, *105* (6), 2117−2122.
(33) Martin, F. P. J.; Dumas, M. E.; Wang, Y. L.; Legido-Quigley, C.; Yap, I. K. S.; Tang, H. R.; Zirah, S.; Murphy, G. M.; Cloarec, O.; Lindon, J. C.; Sprenger, N.; Fay, L. B.; Kochhar, S.; van Bladeren, P.; Holmes, E.; Nicholson, J. K. A top-down systems biology view of microbiome-mammalian metabolic interactions in a mouse model. *Mol. Syst. Biol.* **2007**, *3*, 112.
(34) Shaham, O.; Wei, R.; Wang, T. J.; Ricciardi, C.; Lewis, G. D.; Vasan, R. S.; Carr, S. A.; Thadhani, R.; Gerszten, R. E.; Mootha, V. K. Metabolic profiling of the human response to a glucose challenge reveals distinct axes of insulin sensitivity. *Mol. Syst. Biol.* **2008**, *4*, 214.
(35) Makinen, V. P.; Soininen, P.; Forsblom, C.; Parkkonen, M.; Ingman, P.; Kaski, K.; Groop, P. H.; Ala-Korpela, M. ^{1}H NMR metabonomics approach to the disease continuum of diabetic complications and premature death. *Mol. Syst. Biol.* **2008**, *4*, 167.
(36) Zhang, X.; Wang, Y.; Hao, F.; Zhou, X.; Han, X.; Tang, H.; Ji, L. Human serum metabonomic analysis reveals progression axes for glucose intolerance and insulin resistance statuses. *J. Proteome Res.* **2009**, *8* (11), 5188−5195.
(37) Salek, R. M.; Maguire, M. L.; Bentley, E.; Rubtsov, D. V.; Hough, T.; Cheeseman, M.; Nunez, D.; Sweatman, B. C.; Haselden, J. N.; Cox, R. D.; Connor, S. C.; Griffin, J. L. A metabolomic comparison of urinary changes in type 2 diabetes in mouse, rat, and human. *Physiol. Genomics* **2007**, *29* (2), 99−108.
(38) Rees, D. A.; Alcolado, J. C. Animal models of diabetes mellitus. *Diabetic Med.* **2005**, *22* (4), 359−370.
(39) Lenzen, S. The mechanisms of alloxan- and streptozotocin-induced diabetes. *Diabetologia* **2008**, *51* (2), 216−226.
(40) Elsner, M.; Guldbakke, B.; Tiedge, M.; Munday, R.; Lenzen, S. Relative importance of transport and alkylation for pancreatic beta-cell toxicity of streptozotocin. *Diabetologia* **2000**, *43* (12), 1528−1533.
(41) Zhang, S. C.; Gowda, G. A. N.; Asiago, V.; Shanaiah, N.; Barbas, C.; Raftery, D. Correlative and quantitative ^{1}H NMR-based metabolomics reveals specific metabolic pathway disturbances in diabetic rats. *Anal. Biochem.* **2008**, *383* (1), 76−84.
(42) Oresic, M.; Simell, S.; Sysi-Aho, M.; Nanto-Salonen, K.; Seppanen-Laakso, T.; Parikka, V.; Katajamaa, M.; Hekkala, A.; Mattila, I.; Keskinen, P.; Yetukuri, L.; Reinikainen, A.; Lahde, J.; Suortti, T.; Hakalax, J.; Simell, T.; Hyoty, H.; Veijola, R.; Ilonen, J.; Lahesmaa, R.; Knip, M.; Simell, O. Dysregulation of lipid and amino acid metabolism precedes islet autoimmunity in children who later progress to type 1 diabetes. *J. Exp. Med.* **2008**, *205* (13), 2975−2984.
(43) Junod, A.; Lambert, A. E.; Stauffacher, W.; Renold, A. E. Diabetogenic action of streptozotocin: relationship of dose to metabolic response. *J. Clin. Invest.* **1969**, *48* (11), 2129−2139.

(44) Xiao, C.; Hao, F.; Qin, X.; Wang, Y.; Tang, H. An optimized buffer system for NMR-based urinary metabonomics with effective pH control, chemical shift consistency and dilution minimization. *Analyst* **2009**, *134* (5), 916−925.
(45) Nicholson, J. K.; Foxall, P. J.; Spraul, M.; Farrant, R. D.; Lindon, J. C. 750 MHz ^{1}H and ^{1}H−^{13}C NMR spectroscopy of human blood plasma. *Anal. Chem.* **1995**, *67* (5), 793−811.
(46) Dai, H.; Xiao, C.; Liu, H.; Tang, H. Combined NMR and LC−MS analysis reveals the metabonomic changes in Salvia miltiorrhiza Bunge induced by water depletion. *J. Proteome Res.* **2010**, *9* (3), 1460−1475.
(47) Dai, H.; Xiao, C.; Liu, H.; Hao, F.; Tang, H. Combined NMR and LC-DAD-MS analysis reveals comprehensive metabonomic variations for three phenotypic cultivars of Salvia Miltiorrhiza Bunge. *J. Proteome Res.* **2010**, *9* (3), 1565−1578.
(48) Cloarec, O.; Dumas, M. E.; Trygg, J.; Craig, A.; Barton, R. H.; Lindon, J. C.; Nicholson, J. K.; Holmes, E. Evaluation of the orthogonal projection on latent structure model limitations caused by chemical shift variability and improved visualization of biomarker changes in ^{1}H NMR spectroscopic metabonomic studies. *Anal. Chem.* **2005**, *77* (2), 517−526.
(49) Johan, T.; Svante, W. Orthogonal projections to latent structures (O-PLS). *J. Chemom.* **2002**, *16* (3), 119−128.
(50) Li, H.; Ni, Y.; Su, M.; Qiu, Y.; Zhou, M.; Qiu, M.; Zhao, A.; Zhao, L.; Jia, W. Pharmacometabonomic phenotyping reveals different responses to xenobiotic intervention in rats. *J. Proteome Res.* **2007**, *6* (4), 1364−1370.
(51) Fan, T. W. M. Metabolite profiling by one- and two-dimensional NMR analysis of complex mixtures. *Prog. Nucl. Magn. Reson. Spectrosc.* **1996**, *28* (1996), 161−219.
(52) Lubetzki, J. Physiological effects of insulin. *Pathol. Biol.* **1966**, *14* (9), 584−590.
(53) Cline, G. W.; Rothman, D. L.; Magnusson, I.; Katz, L. D.; Shulman, G. I. ^{13}C-nuclear magnetic resonance spectroscopy studies of hepatic glucose metabolism in normal subjects and subjects with insulin-dependent diabetes mellitus. *J. Clin. Invest.* **1994**, *94* (6), 2369−2376.
(54) David, A. B. Branched chain amino acids: (proceedings of branched chain amino acids, a session from the 2nd international symposium advances in clinical nutrition, May 1982). *FEBS Lett.* **1983**, *164* (1), 203−203.
(55) Hollis, T. M.; Kern, J. A.; Enea, N. A.; Cosgarea, A. J. Changes in plasma histamine concentration in the streptozotocin-diabetic rat. *Exp. Mol. Pathol.* **1985**, *43* (1), 90−96.
(56) Gill, D. S.; Barradas, M. A.; Fonseca, V. A.; Dandona, P. Plasma histamine concentrations are elevated in patients with diabetes mellitus and peripheral vascular disease. *Metabolism* **1989**, *38* (3), 243−247.
(57) de Zwart, L. L.; Meerman, J. H.; Commandeur, J. N.; Vermeulen, N. P. Biomarkers of free radical damage applications in experimental animals and in humans. *Free Radical Biol. Med.* **1999**, *26* (1−2), 202−226.
(58) Suyama, K.; Akagawa, M.; Sasaki, T. Oxidative deamination of lysine residue in plasma protein from diabetic rat: alpha-dicarbonyl-mediated mechanism. *Int. Congr. Ser.* **2002**, *1245*, 243−248.
(59) Wilcken, D. E.; Sim, A. S.; Wang, J.; Wang, X. L. Asymmetric dimethylarginine (ADMA) in vascular, renal and hepatic disease and the regulatory role of L-arginine on its metabolism. *Mol. Genet. Metab.* **2007**, *91* (4), 309−317.
(60) Altinova, A. E.; Arslan, M.; Sepici-Dincel, A.; Akturk, M.; Altan, N.; Toruner, F. B. Uncomplicated type 1 diabetes is associated with increased asymmetric dimethylarginine concentrations. *J. Clin. Endocrinol. Metab.* **2007**, *92* (5), 1881−1885.
(61) Sosenko, J. M.; Kato, M.; Soto, R.; Goldberg, R. B. Plasma lipid levels at diagnosis in type 2 diabetic patients. *Diabetic Med.* **1993**, *10* (9), 814−819.
(62) Obrosova, I. G.; Stevens, M. J.; Lang, H. J. Diabetes-induced changes in retinal NAD-redox status: pharmacological modulation and implications for pathogenesis of diabetic retinopathy. *Pharmacology* **2001**, *62* (3), 172−180.
(63) Armstrong, R. B.; Ianuzzo, C. D. Decay of succinate dehydrogenase activity in rat skeletal muscle following streptozotocin injection. *Horm. Metab. Res.* **1976**, *8* (5), 392−394.
(64) Mackerer, C. R.; Mehlman, M. A.; Tobin, R. B. alpha-Oxoglutarate carboxylation in liver mitochondria from normal, alloxan diabetic and streptozotocin diabetic rats. *Proc. Soc. Exp. Biol. Med.* **1972**, *139* (1), 24−27.
(65) Tancrede, G.; Rousseau-Migneron, S.; Nadeau, A. Long-term changes in the diabetic state induced by different doses of streptozotocin in rats. *Br. J. Exp. Pathol.* **1983**, *64* (2), 117−123.
(66) Phipps, A. N.; Stewart, J.; Wright, B.; Wilson, I. D. Effect of diet on the urinary excretion of hippuric acid and other dietary-derived aromatics in rat. A complex interaction between diet, gut microflora and substrate specificity. *Xenobiotica* **1998**, *28* (5), 527−537.
(67) Marchesi, J. R.; Holmes, E.; Khan, F.; Kochhar, S.; Scanlan, P.; Shanahan, F.; Wilson, I. D.; Wang, Y. Rapid and noninvasive metabonomic characterization of inflammatory bowel disease. *J. Proteome Res.* **2007**, *6* (2), 546−551.
(68) Tian, Y.; Zhang, L.; Wang, Y.; Tang, H. Age-related topographical metabolic signatures for the rat gastrointestinal contents. *J. Proteome. Res.* **2011**, *11* (2), 1397−1411.
(69) Xu, J.; Zhang, L.; Chou, A.; Allaby, T.; Belanger, G.; Radziuk, J.; Jasmin, B. J.; Miki, T.; Seino, S.; Renaud, J. M. KATP channel-deficient pancreatic beta-cells are streptozotocin resistant because of lower GLUT2 activity. *Am. J. Physiol.: Endocrinol. Metab.* **2008**, *294* (2), E326−335.
(70) Thyssen, S.; Arany, E.; Hill, D. J. Ontogeny of regeneration of beta-cells in the neonatal rat after treatment with streptozotocin. *Endocrinology* **2006**, *147* (5), 2346−2356.